Diffusion and defect reactions between donors, C, and vacancies in Ge. I. Experimental results

S. Brotzmann and H. Bracht*
Institute of Material Physics, University of Münster, Wilhelm-Klemm-Strasse 10, D-48149 Münster, Germany

J. Lundsgaard Hansen and A. Nylandsted Larsen
Department of Physics and Astronomy, University of Aarhus, DK-8000 Aarhus, Denmark

E. Simoen
IMEC, Kapeldreef 75, B-3001 Leuven, Belgium

E. E. Haller
University of California at Berkeley and Lawrence Berkeley National Laboratory, 1 Cyclotron Road, Berkeley, California 94720, USA

J. S. Christensen
Department of Physics, University of Oslo, NO-0316 Oslo, Norway

P. Werner
Max-Planck Institute of Microstructure Physics, D-06120 Halle, Germany
(Received 19 February 2008; revised manuscript received 19 May 2008; published 16 June 2008)

The diffusion of self-atoms and *n*-type dopants such as phosphorus, arsenic, and antimony in germanium was studied by means of isotopically controlled multilayer structures doped with carbon. The diffusion profiles reveal an aggregation of the dopants within the carbon-doped layers and a retarded penetration depth compared to dopant diffusion in high-purity natural Ge. Dopant aggregation and diffusion retardation are strongest for Sb and similar for P and As. In addition, the shape of the dopant profiles changes for dopant concentrations in the range of 10^{20} cm^{-3} mainly due to the formation of dopant-vacancy complexes, which is more significant at high concentrations. Accurate modeling of the simultaneous self-diffusion and dopant diffusion is achieved on the basis of the vacancy mechanism and additional reactions that take into account the formation of neutral carbon-vacancy-dopant and neutral dopant-vacancy complexes. The stability of these complexes is compared to theoretical calculations published recently and to additional calculations presented in Part II. The overall consistency between the experimental and theoretical results supports the stabilization of donor-vacancy complexes in Ge by the presence of carbon and the dopant deactivation via the formation of dopant-vacancy and carbon-vacancy-dopant complexes.

DOI: 10.1103/PhysRevB.77.235207 PACS number(s): 61.72.jd, 61.72.uf, 61.72.Yx, 66.70.Df

I. INTRODUCTION

The continuing decrease in the lateral and vertical dimensions of electronic devices requires the formation of ultrashallow junctions with high electrically active dopant concentrations. At present, a renewed interest in germanium (Ge) exists for commercial fabrication of Ge-based field-effect transistors.[1] This trend is driven by the higher carrier mobility in Ge compared to that in silicon (Si) and the development of high-*k* dielectrics as insulating layers on Ge. Whereas implantation of boron (B) in Ge and subsequent annealing[2–4] result in active dopant concentrations of a few 10^{20} cm^{-3}, it still remains difficult to get equivalently high donor concentrations in Ge.[2,4–6] The enhanced diffusion of *n*-type dopants under extrinsic conditions hampers the formation of ultrashallow junctions.[5,7–9] Recently, we have demonstrated that the enhanced diffusion is directly related to the formation and mobility of singly negatively charged dopant-vacancy pairs.[10,11] On the other hand, the slow diffusion of B in Ge favors the formation of ultrashallow p^+/n junctions. This slow diffusion is a consequence of a self-interstitial–mediated B diffusion mechanism.[12] In order to realize ultrashallow *n*-type dopant profiles with high active dopant concentrations, both the enhanced diffusion under extrinsic conditions and the deactivation of the dopant atoms at high concentrations must be controlled. Recently, Luo *et al.*[7] reported that the diffusion of phosphorus (P) in Ge is suppressed by the incorporation of carbon (C). Coimplantation of C and P in Si has also been demonstrated to effectively suppress the diffusion of P in Si.[13] Luo *et al.*[7] argued that the suppression of P diffusion in Ge depends on the same mechanisms that control the suppression of dopant diffusion in C-doped Si[14] and proposed that P in Ge diffuses via a self-interstitial–mediated mechanism.[7] This interpretation, however, is at variance with more recent observations of the diffusion behavior of P in Ge.[11]

In this work, we report experiments on the diffusion of P, arsenic (As), and antimony (Sb) in high-purity natural Ge and isotopically controlled Ge multilayer structures doped with the isovalent impurity C. The presence of C suppresses the diffusion of the *n*-type dopants, but leaves Ge self-diffusion unaffected. The doping dependence of self-diffusion reveals the existence of doubly negatively charged vacancies. Both the self-atom profile and the dopant profile provide evidence of dopant deactivation at high doping levels. Accurate modeling of the experimental profiles supports

 ©2008 The American Physical Society

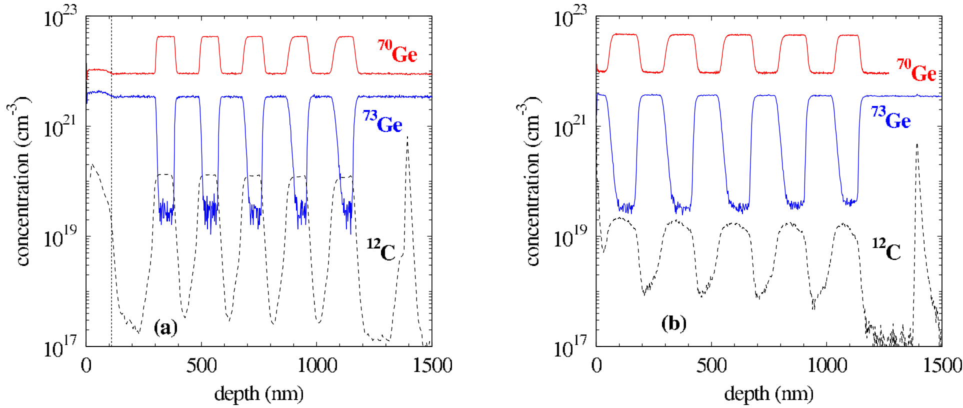

FIG. 1. (Color online) SIMS concentration profiles of ^{70}Ge, ^{73}Ge, and ^{12}C of the as-grown Ge isotope multilayer structure with (a) and without (b) an amorphous Ge cap layer. The position of the amorphous/crystalline Ge interface is indicated by the fine dashed line in (a).

the formation of neutral carbon-vacancy-dopant and neutral dopant-vacancy complexes, whose existence is supported by recent *ab initio* calculations[15–19] and additional calculations presented in Part II.

II. EXPERIMENT

(100)-oriented *p*-type single-crystalline Ge wafers (>30 Ω cm) with a thickness of about 500 μm and isotope heterostructures grown by means of molecular beam epitaxy (MBE) at 400 °C on a (100)-oriented ^{nat}Ge substrate wafer were used for the diffusion experiments. The isotope structure consists of an amorphous Ge capping layer, which is about 100 nm thick, followed by a 200-nm-thick crystalline ^{nat}Ge layer and subsequent ten alternating layers of about 100-nm-thick ^{70}Ge and about 100-nm-thick ^{nat}Ge. The isotopically enriched ^{70}Ge layers were doped with C to concentrations of about 10^{20} cm^{-3}. Another MBE-grown Ge isotope structure used for the diffusion experiments consists of ten alternating ^{nat}Ge and ^{70}Ge layers without an amorphous capping layer. The ^{70}Ge layers of this structure were doped with C to about 10^{19} cm^{-3}. The dopants of interest were either implanted into the top amorphous Ge layer utilizing primary energies (doses) of 35 keV ($1.0E+16$ cm^{-2}), 80 keV ($1.0E+16$ cm^{-2}), and 470 keV ($7.0E+15$ cm^{-2}) for P, As, and Sb implantation, respectively, or diffused into the isotope structure from the gas phase. The implanted top layer serves as dopant source during diffusion annealing. Samples with lateral dimensions of 5×5 mm^2 were cut from the wafers. A Ge-dopant alloy source with about 1 at. % dopant content was prepared by melting elemental Ge and the respective amount of the elemental dopant in a closed ampoule. Both Ge isotope and natural Ge samples were encapsulated in an evacuated quartz ampoule together with several milligrams of the Ge-dopant alloy. The alloy source effectively prevents depletion of the dopants within the implanted amorphous Ge layer of the isotope structure and serves as infinite dopant source for diffusion experiments with isotope structures without an implanted amorphous cap layer. Diffusion anneals were performed at temperatures ranging between 600 and 750 °C in a resistance heated furnace for times between 9 h and 15 min that ensure a dopant profile within the isotope structure. In order to ensure a fast ramping up to the desired diffusion temperature, the ampoules were inserted into a preheated furnace. A type-*S* Pt-PtRh thermocouple was used to monitor the temperature within an accuracy of ±2 K. The ampoules were quenched in ethylene glycol to terminate the diffusion process. The dopant profiles were measured by means of secondary-ion-mass spectrometry (SIMS). The SIMS measurements were performed with a Cameca system using oxygen as a primary ion beam. Dopant- and C-implanted Ge reference samples with a maximum dopant concentration of 1.0×10^{19} cm^{-3} were used for the calibration of the SIMS signal. The depths of the craters left from the SIMS analysis were determined with a Talystep profilometer.

III. RESULTS

Figures 1(a) and 1(b) show the SIMS concentration profiles of ^{70}Ge, ^{73}Ge, and ^{12}C of the as-grown Ge isotope structure with and without an amorphous Ge cap layer, respectively. The SIMS analysis of the former structure reveals a C concentration within the ^{70}Ge layers of about 10^{20} cm^{-3}, whereas the ^{70}Ge layers of the latter sample contain about 10^{19} cm^{-3} carbon. Annealing at 600 and 700 °C without exposure to a dopant source leads to a homogeneous broadening of the isotope structure.[20] The broadening is accurately described with the Ge diffusion coefficient reported by Werner *et al.*[21] for intrinsic conditions. This shows that self-diffusion is not affected by the presence of C in the ^{70}Ge layers. The C distribution itself does not change within the temperature and time window covered by the experiments. This indicates that C diffusion in Ge is significantly slower than self-diffusion and presumably, like B, is also mediated by self-interstitials. Figures 2–4 illustrate P, As, and Sb diffusion profiles and the corresponding Ge and C profiles in Ge isotope heterostructures after annealing at temperatures between 600 and 750 °C. The dopant profiles that are established in the case where an implanted amorphous cap layer serves as dopant source are characterized by a high doping level of 10^{21} cm^{-3} within the first 100 nm from the surface. The dopant profiles in samples without an amorphous cap layer were obtained by means of the Ge-dopant alloy source that maintains a constant vapor pressure within the closed diffusion ampoule. For comparison, dopant profiles in natural Ge established at the same temperature and time are also shown in Figs. 2–4. The dopant diffusion is independent of

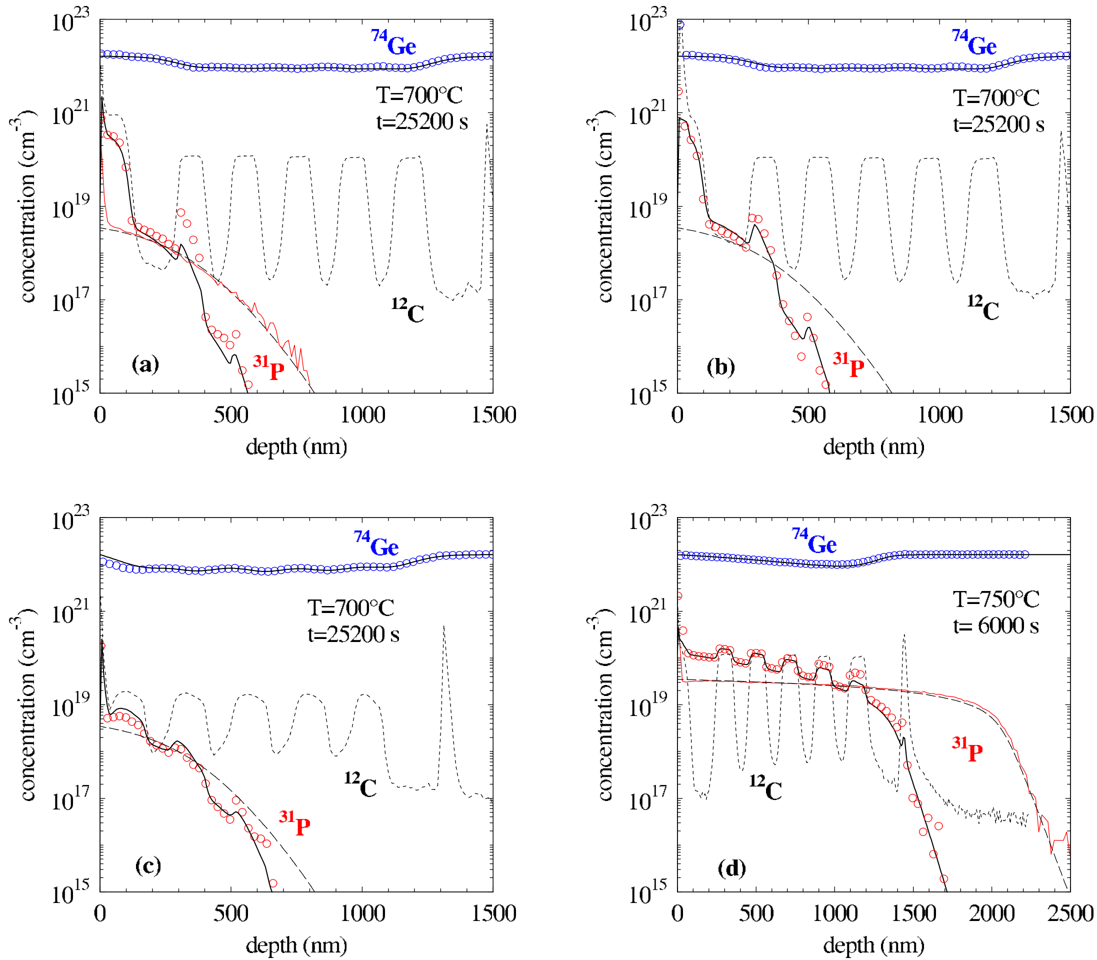

FIG. 2. (Color online) Concentration profiles of ^{31}P (lower symbols), ^{74}Ge (upper symbols), and ^{12}C (short dashed line) measured with SIMS after diffusion annealing of the Ge isotope multilayer structures at the temperatures and times indicated (structures with (without) amorphous cap layer: (a), (b), and (d) [(c)]). The isotope structures illustrated in (a)–(c) were annealed in the same diffusion ampoule together with a natural Ge sample and a GeP alloy source. Under these conditions almost identical P profiles were obtained for a P-implanted (b) and not implanted (a) Ge isotope structure. The experimental P profiles (thin solid lines) established in natural Ge under identical conditions are shown for comparison in (a) and (d). The black upper and lower solid lines are best fits to the experimental ^{74}Ge and ^{31}P profiles in the Ge isotope structure calculated on the basis of reactions (1)–(3). The thin wide dashed lines are best fits to the P profiles in natural Ge that are also shown in (b) and (c) representative for the experimental profile already illustrated in (a). Carbon doping of the Ge isotope structure yields to a suppression of P diffusion compared to P diffusion in high-purity natural Ge. The carbon distribution remained unchanged after diffusion annealing.

the dopant source realized in our experiments [see Figs. 2(a) and 2(b)]. Therefore, in the following we do not differentiate between dopant profiles obtained with the implanted dopant source and the Ge-dopant alloy source.

The self-diffusion profiles illustrated in Figs. 2–4 reveal an enhanced intermixing of the ^{nat}Ge/^{70}Ge layers within the P, As, and Sb profiles, respectively. This, in particular, becomes evident in the As and Sb diffusion experiments. The self-diffusion is largest close to the surface and lowest at the front of the dopant profiles. This doping dependence indicates that Ge self-diffusion is mediated by acceptor-like negatively charged native defects. In order to determine the charge state of the defect, the doping dependence of self-diffusion must be analyzed more quantitatively (see below).

The dopant profiles exhibit a peculiar concentration "stepup" in each ^{70}Ge layer of the as-grown structure. For comparison, the profiles in natural Ge show the expected box shape.[11] The dopant stepup in the Ge isotope structure appears along a reduced penetration depth compared to the profiles in natural Ge (see Figs. 2–4). The aggregation of dopants and suppression of their diffusivity in the isotope structure are characteristic for a trap-limited diffusion. It is evident from Figs. 2–4 that the C distribution of the isotope structure not only remains unaffected by annealing but also correlates with the dopant stepup. Obviously, the dopant aggregation is caused by C. The high C concentration of about 10^{20} cm^{-3} exceeds the solubility in Ge by several orders of magnitude.[22] Investigations of the microstructure by means of cross-section transmission electron microscopy (TEM) did not show any C precipitates in the single-crystalline Ge epitaxial layers either in the as-grown or annealed isotope structures. This is demonstrated by the TEM picture in Fig. 5. The TEM analysis reveals a recrystallization of the amorphous Ge layer upon annealing and small precipitates of a few

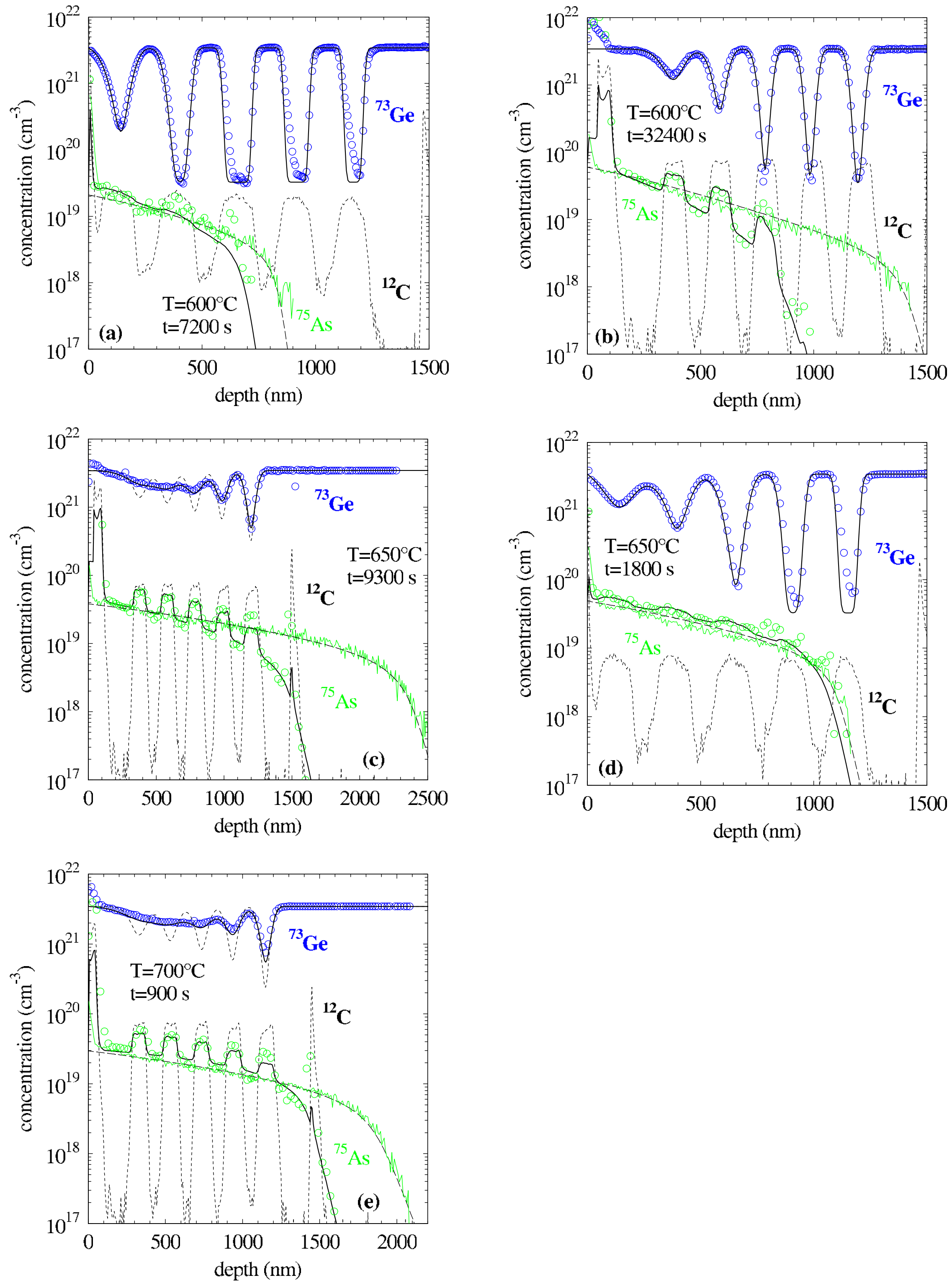

FIG. 3. (Color online) Concentration profiles of ^{75}As (lower symbols), ^{73}Ge (upper symbols), and ^{12}C (lower short dashed line) measured with SIMS after diffusion annealing of the Ge isotope multilayer structures at the temperatures and times indicated (structures with (without) amorphous cap layer: (b), (c), and (e) [(a) and (d)]). The experimental As profiles (thin solid lines) established in natural Ge under identical diffusion conditions are shown for comparison. It is evident that carbon doping of the Ge isotope structure leads to a suppression of As diffusion compared to As diffusion in high-purity natural Ge. The upper and lower black solid lines are best fits to the experimental ^{74}Ge and ^{31}P profiles in the Ge isotope structure calculated on the basis of reactions (1)–(3). The thin wide dashed lines show best fits to the As profiles in natural Ge. The upper short dashed lines in (c) and (e) show simulations of the simultaneous As diffusion and self-diffusion for the case where the vacancies are singly negatively charged as proposed by Werner et al. (Ref. 21).

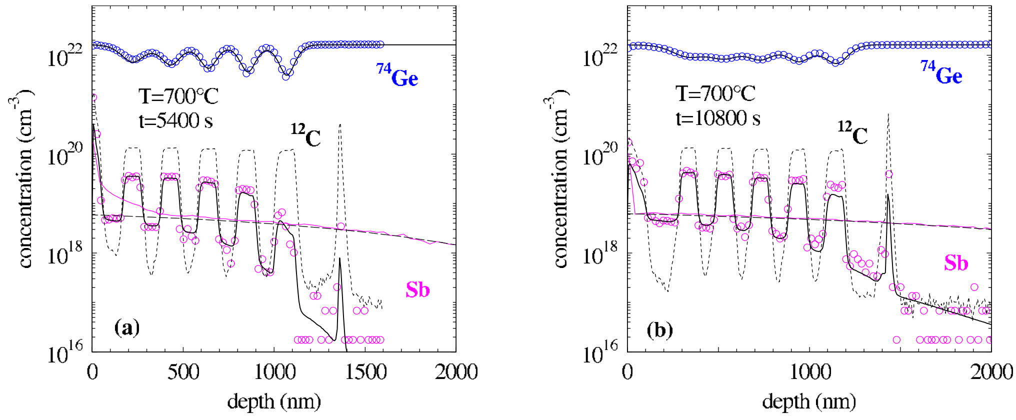

FIG. 4. (Color online) Concentration profiles of Sb (lower symbols), ^{74}Ge (upper symbols), and ^{12}C (lower short dashed line) measured with SIMS after diffusion annealing of the Ge isotope multilayer structure with amorphous cap layer at the temperatures and times indicated. The experimental Sb profiles (thin solid lines) established in natural Ge under identical diffusion conditions are shown for comparison. The presence of carbon in the Ge isotope structure strongly suppresses the diffusion of Sb. The upper and lower black solid lines are best fits to the experimental ^{74}Ge and Sb profiles in the Ge isotope structure calculated on the basis of reactions (1)–(3). The thin wide dashed lines show best fits to the Sb profiles in natural Ge. Note that diffusion annealing did not change the carbon distribution in the isotope structure.

nanometers in diameter close to the single-crystalline/polycrystalline interface. The high-resolution image of the precipitates shown in the inset of Fig. 5 indicates the crystalline and coherent nature of the precipitates that very likely are related to GeAs phases. No evidence of carbon precipitates was found in this and other samples. Therefore, we assume that C is mainly incorporated on substitutional sites. This assumption is supported by recent investigations on the lattice site distribution of C in epitaxially grown $Ge_{1-y}C_y$/Ge layers.[23] At C concentrations of $y \lesssim 0.003$, a substantial amount of C is incorporated on substitutional sites. According to the results of D'Arcy-Gall *et al.*,[23] C with a concentration of 10^{20} cm^{-3} in the ^{70}Ge layers, i.e., $y \approx 0.002$, can be mainly dissolved on substitutional sites. This is also supported by the theoretical calculations presented in Part II. Both the low diffusivity of C and metastability of CC pairs prohibits the formation of larger carbon clusters.

It is noticeable that the shape of the dopant profile changes to being less box shaped in the case where the dopant concentration is close to 10^{20} cm^{-3}. This becomes obvious in the shape of the P profile in the Ge isotope multilayer structure compared to the profile in natural Ge [see, e.g., Fig. 2(d)]. In natural Ge the expected box-shaped P profile is established at a maximum doping level of about 3×10^{19} cm^{-3}. A far less pronounced box shape of the P profile for concentrations close to 10^{20} cm^{-3} is obtained in the isotope structure. This change in profile shape is at variance with the diffusion behavior of n-type dopants in Ge expected on the basis of the vacancy mechanism,[11]

$$(AV)^- \rightleftarrows A_s^+ + V^{2-}, \quad (1)$$

with $A \in \{P, As, Sb\}$. In Eq. (1) AV, A_s, and V are the dopant-vacancy pair, the substitutional dopant, and the vacancy, respectively. The charge states of the defects are indicated by the superscripts. To model the trapping of n-type dopants within the carbon-doped layers and the change in the shape of the dopant profiles for high dopant concentrations, the following reactions are assumed in addition to Eq. (1):

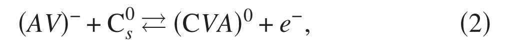

$$(AV)^- + C_s^0 \rightleftarrows (CVA)^0 + e^-, \quad (2)$$

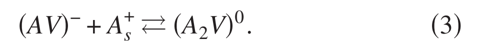

$$(AV)^- + A_s^+ \rightleftarrows (A_2V)^0. \quad (3)$$

Equation (2) accounts for the trapping of mobile AV^- pairs within the C-doped Ge layers by forming CVA complexes. This reaction leads to a reduction in strain energy. The complex formation effectively reduces the tensile strain that is associated with the incorporation of C on substitutional site. Equation (3) describes the formation of neutral dopant-vacancy complexes $(A_2V)^0$ that are favored by Coulomb attraction of the opposite charged defects $(AV)^-$ and A_s^+. The complexes $(CVA)^0$ and $(A_2V)^0$ are both considered immobile relative to the mobile $(AV)^-$ pairs. The charge states assigned to the various defects follow from the demand to accurately describe both the dopant and self-atom profiles. The CVA and A_2V complexes appear to be electrically neutral under the conditions realized by the diffusion experiments.

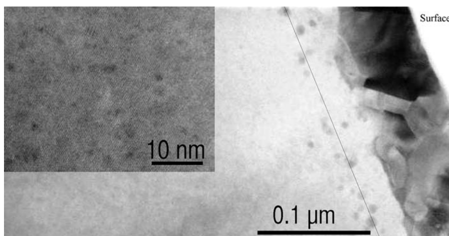

FIG. 5. Cross-section TEM image of a Ge isotope sample diffused with As at 700 °C for 900 s. The corresponding SIMS profiles are illustrated in Fig. 3(e). The TEM analysis reveals a recrystallization of the initial 100-nm-thick amorphous Ge layer and a zone of small precipitates close to the single-crystalline/polycrystalline interface. These precipitates are crystalline and coherent as illustrated by the high-resolution image (see inset) and very likely consist of a Ge-As phase. The positions of the single-crystalline/polycrystalline interface (thin solid line) and the surface of the sample are indicated.

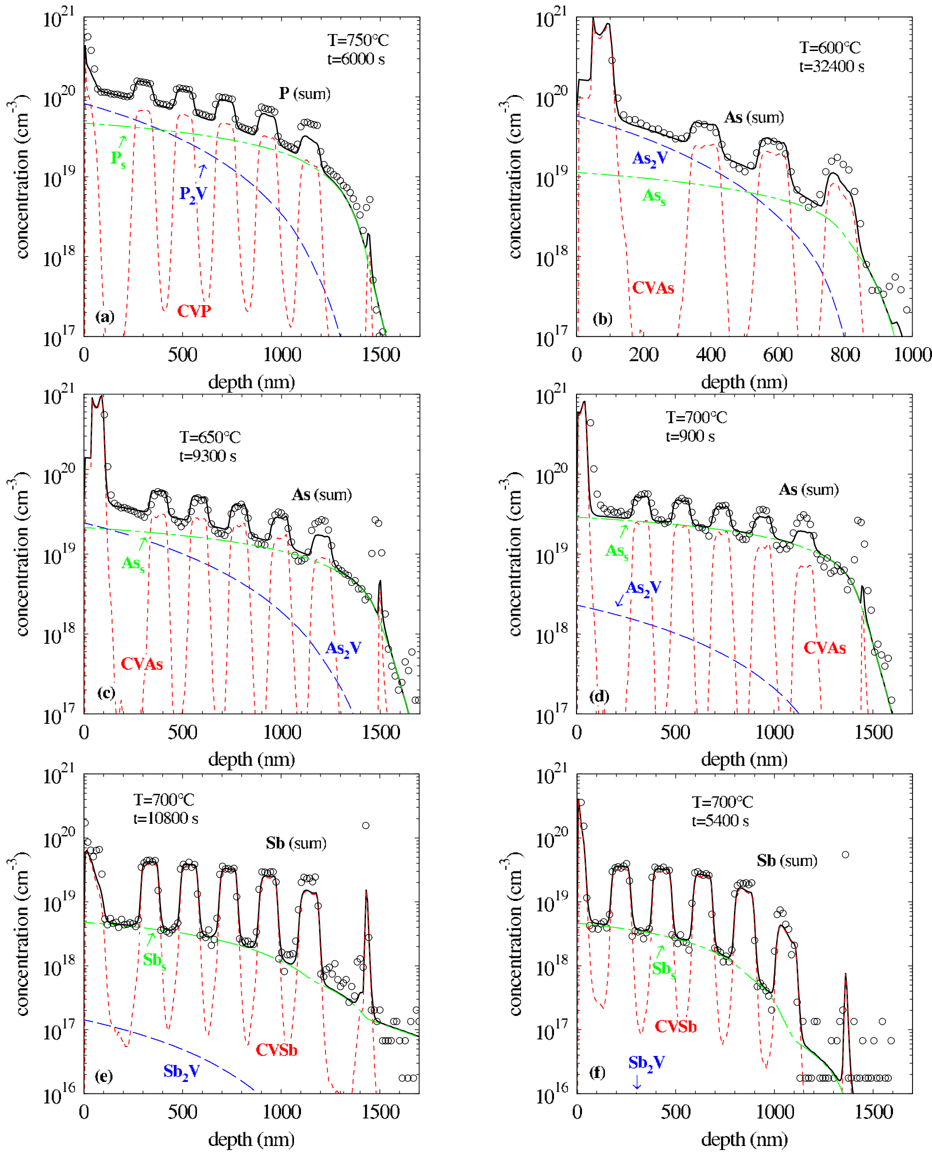

FIG. 6. (Color online) Contributions of A_s (chain dotted line), CVA (short dashed line), and A_2V (long dashed line) with $A \in \{P, As, Sb\}$ to the total dopant concentration (black solid line) that accurately describe the SIMS concentration profiles (symbols) [(a): P; (b)–(d): As; (e) and (f): Sb].

Best fits to the experimental profiles are illustrated by the solid lines in Figs. 2–4. The simulations on the basis of reactions (1)–(3) accurately describe the diffusion behavior of the n-type dopants in natural high-purity Ge and the simultaneous self- and dopant diffusion in C-doped Ge isotope heterostructures. In the framework of reactions (1)–(3), the fitting is unique with respect to the charge states of the vacancy, the C trapping center C_s^0, the carbon-vacancy-dopant CVA complex, and the dopant-defect A_2V complex in reaction (3). Figures 3(c) and 3(e) demonstrate simulations of the simultaneous self-diffusion and dopant diffusion assuming that all vacancies are singly negatively charged (upper dashed lines) and doubly negatively charged (upper solid lines). Taking into account the intrinsic Ge self-diffusion coefficient determined by Werner *et al.*,[21] the doping enhanced Ge self-diffusion is best described with doubly negatively charged vacancies.

The nature of the C- and dopant-related defects cannot be determined unambiguously from the experimental profiles. However, recent *ab initio* calculations support the formation of dopant-vacancy[15,16,18,19] and carbon-vacancy-dopant[17] complexes. In Part II more comprehensive theoretical calculations on the association of C with n-type dopants P, As, and Sb are presented that provide details about the structure, stability, and mobility of the carbon-vacancy-dopant complexes in Ge.

The simulation of dopant diffusion on the basis of Eqs. (1)–(3) provides the concentration profiles of the individual dopant-related defects. Figures 6(a)–6(f) demonstrate the individual contributions that add up to the total dopant profile measured with SIMS. In the case of As diffusion, the contribution of As_2V complexes to the total As concentration decreases with increasing temperature [see Figs. 6(b)–6(d)], whereas in the case of P the contribution of P_2V remains significant even at 750 °C [see Fig. 6(a)]. Compared to P and As, the formation of Sb_2V complexes is not significant and can be neglected for detailed modeling of Sb diffusion in Ge [see Figs. 6(e) and 6(f)]. In accord with our previous results on intrinsic and extrinsic diffusion of P, As, and Sb in Ge,[11] the concentration of AV^- pairs is considered to be several orders of magnitude lower than the maximum donor concentration $C^{eq}_{A_s^+}$, i.e., $C^{eq}_{AV^-}/C^{eq}_{A_s^+} \ll 10^{-5}$. Hence, AV^- pairs

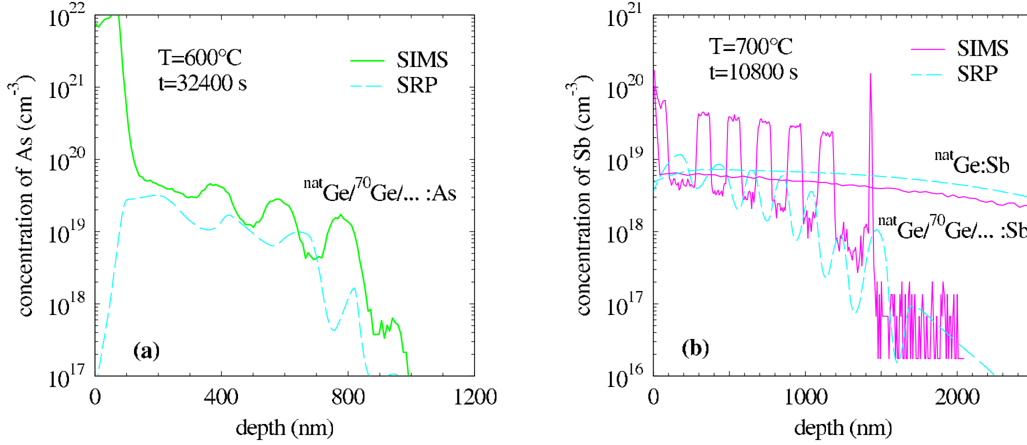

FIG. 7. (Color online) Concentration profiles of As (a) and Sb (b) measured by means of SIMS and nano-SRP. Within the accuracy of the electrical profiling technique, the SRP and SIMS profiles of Sb in natural Ge are in good agreement [see upper dashed and solid lines in (b)]. The electrical and chemical dopant profiles in the carbon-doped isotope structures deviate from each other [see (a) and (b)]. This deviation is attributed to differences in the electron mobilities between the carbon-doped ^{70}Ge and the undoped ^{nat}Ge layers.

do not contribute to the total concentration of A.

In addition to SIMS measurements that provide information about the chemical concentration of the n-type dopants, some dopant-diffused isotope structures were analyzed by means of nanospreading-resistance profiling (nano-SRP).[24] Figures 7(a) and 7(b) show a comparison of the concentration profiles of As and Sb, respectively, measured with SIMS and nano-SRP after diffusion annealing. Figure 7(b) demonstrates that the electrical active concentration of Sb in natural Ge is in good agreement with the chemical profile measured with SIMS. In contrast, the nano-SRP measurements of the As- and Sb-diffused Ge isotope structures illustrated in Figs. 7(a) and 7(b) reveal an undulating shape of the electrical profile. The local maxima of the electrical profile correlate with the natural Ge layers rather than with the heavily C-doped layers. On first sight the electrical profile seems to suggest that the concentration of electrically active dopants within the C-doped layers is lower than in the natural Ge layers not doped with C. If this were true, self-diffusion should be affected by an undulating free-electron concentration. However, the doping enhanced self-diffusion indicates a gradual change in the free carrier concentration rather than an undulating run. This reveals that the undulating shape of the nano-SRP profile is more likely caused by different mobilities of the free carriers within the C-doped and undoped Ge layers. The different carrier mobilities are a consequence of the stronger scattering of the free carriers within the C-doped layers compared to the undoped Ge. Accordingly, the free carriers within the C-doped layers possess a lower mobility than in undoped Ge.

Isotope structures with about 1 order of magnitude lower C content ($\approx 10^{19}$ cm^{-3}) show a less pronounced aggregation of P and As within the C-doped Ge layers and a lower suppression of dopant diffusion compared to the samples with high C concentration. This is demonstrated by the P and As profiles in Figs. 2(c), 3(a), and 3(d). Nano-SRP measurements of the same samples yield donor profiles that are in good agreement with the chemical profiles (not shown). The weak correlation of the electrical profile with the distribution of C is in accord with the reduced C concentration.

The intrinsic diffusion coefficient $D_A(n_{in})$ with $A \in \{\mathrm{P}, \mathrm{As}, \mathrm{Sb}\}$ deduced from fitting the experimental dopant profiles shown in Figs. 2–4 are listed in Table I and illustrated in Fig. 8. The results are in good agreement with the Arrhenius expressions of the intrinsic diffusion coefficients,

$$D_{\mathrm{P}}(n_{\mathrm{in}}) = 9.1^{+5.3}_{-3.4} \exp\left[-\frac{(2.85 \pm 0.04)\ \mathrm{eV}}{k_B T}\right] \ \mathrm{cm}^2\ \mathrm{s}^{-1}, \tag{4}$$

$$D_{\mathrm{As}}(n_{\mathrm{in}}) = 32^{+21}_{-13} \exp\left[-\frac{(2.71 \pm 0.06)\ \mathrm{eV}}{k_B T}\right] \ \mathrm{cm}^2\ \mathrm{s}^{-1}, \tag{5}$$

$$D_{\mathrm{Sb}}(n_{\mathrm{in}}) = 16.7^{+6.6}_{-4.7} \exp\left[-\frac{(2.55 \pm 0.03)\ \mathrm{eV}}{k_B T}\right] \ \mathrm{cm}^2\ \mathrm{s}^{-1}, \tag{6}$$

that were recently determined from intrinsic and extrinsic dopant diffusion experiments in natural Ge.[11] Within the experimental accuracy, the data for the intrinsic carrier concentration n_{in} determined in this work (see Table I) and in a recent publication[11] are in good agreement. The scatter in the data of n_{in} reflects the accuracy of the SIMS technique to determine absolute dopant concentrations.[11] Fitting of the experimental profiles provides data for the carbon-vacancy-dopant and dopant-vacancy complexes. The model parameter $C_{\mathrm{C}}^{\mathrm{eff}}$ considers the amount of C that effectively acts as trapping center. This parameter may depend on the type of dopant and temperature.

IV. DISCUSSION

The continuum theoretical calculation of the simultaneous self-diffusion and dopant diffusion are sensitive to the charge states of the defects involved in reactions (1)–(3) rather than

TABLE I. Intrinsic diffusion coefficient $D_A(n_{in})$ $[\equiv D^*_{(AV)^-}(n_{in})^{11}]$ of the n-type dopant $A \in \{P, As, Sb\}$ in Ge determined from modeling the interference between self-diffusion and dopant diffusion in Ge isotope multilayer structures and from modeling dopant diffusion in natural Ge on the basis of reactions (1)–(3). The corresponding diffusion temperature T and time t, maximum donor concentration $C^{eq}_{A_s^+}$, intrinsic carrier concentration n_{in}, total effective carbon concentration C^{eff}_C, and concentration of carbon-vacancy-dopant C^{eq}_{CVA}, and dopant-vacancy complexes $C^{eq}_{A_2V}$ in thermal equilibrium are also listed. The subscript of the dopant element indicates the Ge material used in the diffusion experiment.

Dopant A	T (°C)	t (s)	$C^{eq}_{A_s^+}$ (cm^{-3})	n_{in} (cm^{-3})	$D_A(n_{in})$ (cm^2 s^{-1})	C^{eff}_C (cm^{-3})	C^{eq}_{CVA} (cm^{-3})	$C^{eq}_{A_2V}$ (cm^{-3})
P[a]	700	25 200	9.1×10^{18}	4.4×10^{18}	1.3×10^{-14}	1.3×10^{20}	4.5×10^{19}	1.4×10^{18}
P[b]	700	25 200	2.7×10^{18}	3.8×10^{18}	1.6×10^{-14}	2.0×10^{19}	8.0×10^{18}	4.1×10^{17}
P[a]	700	25 200	9.1×10^{18}	4.4×10^{18}	1.3×10^{-14}	1.3×10^{20}	4.5×10^{19}	1.3×10^{18}
P[a]	750	6 000	4.7×10^{19}	7.4×10^{18}	5.5×10^{-14}	1.3×10^{20}	7.6×10^{19}	4.1×10^{19}
As[b]	600	72 00	1.0×10^{19}	1.8×10^{18}	1.4×10^{-14}	2.0×10^{19}	3.6×10^{18}	7.2×10^{18}
As[c]	600	72 00	1.0×10^{19}	1.4×10^{18}	8.4×10^{-15}			5.4×10^{18}
As[a]	600	32 400	1.1×10^{19}	1.7×10^{18}	9.0×10^{-15}	3.5×10^{19}	2.9×10^{19}	2.9×10^{19}
As[c]	600	32 400	1.2×10^{19}	1.5×10^{18}	6.2×10^{-15}			2.4×10^{19}
As[a]	650	9 300	2.1×10^{19}	3.5×10^{18}	4.7×10^{-14}	5.5×10^{19}	3.4×10^{19}	1.2×10^{19}
As[c]	650	9 300	1.9×10^{19}	2.8×10^{18}	6.2×10^{-14}			9.6×10^{18}
As[b]	650	1 800	2.8×10^{19}	3.7×10^{18}	5.8×10^{-14}	2.0×10^{19}	8.6×10^{18}	1.2×10^{19}
As[c]	650	1 800	2.2×10^{19}	3.0×10^{18}	6.2×10^{-14}			1.3×10^{19}
As[a]	700	900	2.9×10^{19}	3.9×10^{18}	2.3×10^{-13}	7.0×10^{19}	2.9×10^{19}	1.2×10^{18}
As[c]	700	900	1.7×10^{19}	3.0×10^{18}	5.4×10^{-13}			6.3×10^{18}
Sb[a]	700	5 400	4.7×10^{18}	5.0×10^{18}	1.2×10^{-12}	3.7×10^{19}	3.2×10^{19}	
Sb[a]	700	10 800	4.8×10^{18}	5.4×10^{18}	1.0×10^{-12}	3.7×10^{19}	3.1×10^{19}	

[a]Ge isotope structure with a total carbon concentration of about 10^{20} cm^{-3} within the ^{70}Ge layer.
[b]Ge isotope structure with a total carbon concentration of about 10^{19} cm^{-3} within the ^{70}Ge layer.
[c]Natural high-purity Ge.

to their detailed structure. The identification of the defects relies on additional information such as the effect of hydrostatic pressure on self-diffusion. This has demonstrated that the native defect mediating self-diffusion in Ge is the vacancy.[21] The presence of dopant-vacancy pairs and evidence for the vacancy mechanism stem from the analysis of defects formed by particle irradiation[25–28] and dopant diffusion studies.[10,11] The specific defects are supported by *ab initio* calculations that predict the formation of dopant-vacancy pairs[15–18,29] and vacancies in different charge states.[30,31] In addition, theory predicts the formation of more complicated donor-vacancy complexes[19] such as A_xV defects that can explain the limited activation of n-type dopant implants in Ge.[32] For example, As_3V and P_3V complexes in heavily As- and P-doped Si have been identified by means of positron lifetime and coincidence Doppler broadening measurements.[33,34] The formation of these defects explains the observed electrical compensation of Si at high doping levels. It should be noted that along the A_2V complex considered in this paper for heavily doped Ge layers, other vacancy-type defects A_nV, which give rise to acceptor states near the valence band, can form by irradiation of lightly and moderately doped Ge.[35,36]

Equations (4)–(6) reveal activation enthalpies Q_A of 2.85, 2.71, and 2.55 eV for the diffusion of P, As, and Sb via AV pairs. The activation enthalpy of dopant diffusion via the

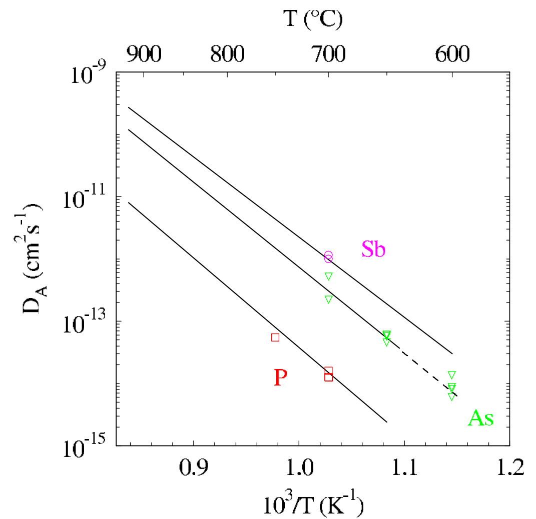

FIG. 8. (Color online) Intrinsic diffusion coefficients of the n-type dopants P, As, and Sb in Ge versus the inverse temperature. The solid lines show the temperature dependence of dopant diffusion for intrinsic conditions determined from intrinsic and extrinsic dopant diffusion studies [see Ref. 11 and Eqs. (4)–(6)]. The dashed line is an extrapolation of Eq. (5) to lower temperatures. The symbols illustrate the data determined in this work from modeling the simultaneous self-diffusion and dopant diffusion in carbon-doped Ge isotope heterostructures and from modeling As diffusion in natural Ge.

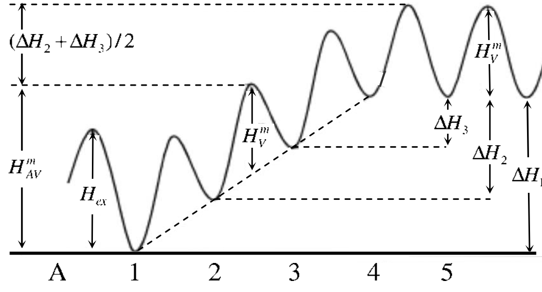

FIG. 9. Potential energy landscape of a vacancy close and far away from a dopant A. H_{AV}^m and H_V^m are the migration enthalpies of the dopant-vacancy pair and the isolated vacancy, respectively. ΔH_1, ΔH_2, and ΔH_3 denote the differences in potential energy between a vacancy far away and those on first-, second-, and third-nearest-neighbor sites from the dopant, respectively. H_{ex} is the enthalpy barrier for site exchange between dopant and vacancy.

vacancy mechanism represents the sum of the formation and migration enthalpy of AV pairs, i.e., $Q_A=H_{AV}^f+H_{AV}^m$. Following the analysis of dopant diffusion via vacancies by Hu,[37] the activation enthalpy can be decomposed as

$$Q_A=\underbrace{H_V^f-\Delta H_1}_{H_{AV}^f}+\underbrace{H_V^m+\Delta H_1-\Delta H_3}_{H_{AV}^m}, \tag{7}$$

where H_V^f and H_V^m are the formation and migration enthalpies of vacancies far away from the dopant. The potential energy landscape of the vacancy as assumed by Hu[37] and Dunham and Wu[38] is illustrated in Fig. 9. ΔH_1, ΔH_2, and ΔH_3 denote the differences in potential energy between a vacancy far away and those on first-, second-, and third-nearest-neighbor sites from the dopant, respectively. The more recent analysis of vacancy-mediated diffusion in a diamond structure performed by Dunham and Wu[38] lead to the following modification of the approach by Hu:[37]

$$Q_A=H_V^f+H_V^m-\frac{\Delta H_2+\Delta H_3}{2}, \tag{8}$$

$$=H_V^f+H_V^m-\overline{\Delta H_{23}}. \tag{9}$$

Equation (8) accounts for a reduction in the migration barrier of the vacancy associated with changes in the binding energy between the sites. Taking into account the activation enthalpy of self-diffusion $Q_{\text{Ge}}=H_V^f+H_V^m=3.09$ eV determined by Werner *et al.*[21] and the activation enthalpy Q_A of dopant diffusion, the differences of $Q_{\text{Ge}}-Q_{\text{P}}=0.24$ eV, $Q_{\text{Ge}}-Q_{\text{As}}=0.38$ eV, and $Q_{\text{Ge}}-Q_{\text{Sb}}=0.54$ eV are obtained. Obviously, the binding energy of the vacancy increases with increasing atomic size of the dopant element. According to Dunham and Wu,[38] the difference $Q_{\text{Ge}}-Q_{\text{A}}$ is the average of the vacancy binding energy $\overline{\Delta H_{23}}$ at the second- and third-nearest-neighbor sites from the dopant with respect to a vacancy far away [see Eqs. (7) and (8)]. For the interactions of P, As, and Sb with a vacancy, respectively, we get $\overline{\Delta H_{23}}=-0.24$, -0.38, and -0.54 eV. The negative energy shows that the pair is more stable than the isolated defects. Recent theoretical calculations of Chroneos *et al.*[17,39] yield -0.52, -0.60, and -0.70 eV for the binding energy of PV, AsV, and SbV pairs, respectively, whereas Coutinho *et al.*[15] obtained a binding energy of -1.05 eV for SbV. Qualitatively, theory predicts the same trend; that is, the binding energy increases with increasing size of the dopant element. However, the calculated energies are higher compared to the experimental results. This apparent discrepancy is related to the fact that the theoretical and experimental binding energies refer to different sites of the vacancy with respect to the dopant. The calculated binding energy refers to the potential energy of a vacancy at first-nearest-neighbor site from the dopant, whereas the binding energy obtained from the experiments refers to a vacancy at second/third nearest position. Accordingly, a direct comparison between experimental and theoretical results is difficult. However, the binding energy of a vacancy next to the dopant atom is certainly higher than the binding energy between dopants and vacancies at second-/third-nearest-neighbor sites. This explains that the calculated binding energies are higher than the experimental values. On the other hand, it is interesting to compare the differences in the binding energy of AV pairs predicted by theory, i.e.,

$$\Delta H_1^{\text{P}V}-\Delta H_1^{\text{As}V}=-0.08 \text{ eV}, \tag{10}$$

$$\Delta H_1^{\text{P}V}-\Delta H_1^{\text{Sb}V}=-0.18 \text{ eV}, \tag{11}$$

$$\Delta H_1^{\text{As}V}-\Delta H_1^{\text{Sb}V}=-0.10 \text{ eV}, \tag{12}$$

to the differences in the binding energy of AV pairs obtained from our experiments

$$(Q_{\text{Ge}}-Q_{\text{P}})-(Q_{\text{Ge}}-Q_{\text{As}})=\overline{\Delta H_{23}^{\text{P}V}}-\overline{\Delta H_{23}^{\text{As}V}}=-0.14 \text{ eV}, \tag{13}$$

$$(Q_{\text{Ge}}-Q_{\text{P}})-(Q_{\text{Ge}}-Q_{\text{Sb}})=\overline{\Delta H_{23}^{\text{P}V}}-\overline{\Delta H_{23}^{\text{Sb}V}}=-0.30 \text{ eV}, \tag{14}$$

$$(Q_{\text{Ge}}-Q_{\text{As}})-(Q_{\text{Ge}}-Q_{\text{Sb}})=\overline{\Delta H_{23}^{\text{As}V}}-\overline{\Delta H_{23}^{\text{Sb}V}}=-0.16 \text{ eV}. \tag{15}$$

The energies given by Eqs. (10)–(15) indicate that the potential energy of a vacancy at a specific site depends on the dopant element. More specifically, Eqs. (10)–(15) describe a shift in the potential energy landscape of the vacancy diffusion pathway in the neighborhood of the dopant. This shift is likely caused by the local stress in the Ge matrix due to the different atomic sizes of the dopants. The calculated and experimental values given by Eqs. (10)–(12) and Eqs. (13)–(15), respectively, not only describe the same trend, but also agree quantitatively within the experimental accuracy of Q_{Ge} and Q_A that in total amount to about 0.1 eV.

The temperature dependence of the ratio $C_{CVA}^{\text{eq}}/C_{A_s}^{\text{eq}}$ between the maximum concentration of the carbon-vacancy-dopant complex and the concentration of the substitutional dopant can be described with $C' \exp(-\Delta H_{CVA}^f/k_BT)$, where ΔH_{CVA}^f is the difference in the formation enthalpy between CVA and A_s. C' is a constant that comprises the formation entropy. Taking into account data of $C_{\text{CVAs}}^{\text{eq}}$ and $C_{\text{As}_s}^{\text{eq}}$ from the analysis of As diffusion in the Ge isotope structure with a

carbon concentration of about 10^{20} cm^{-3} (see Table I), the temperature dependence of $C^{\mathrm{eq}}_{\mathrm{CVAs}}/C^{\mathrm{eq}}_{\mathrm{As}_s}$ yields $\Delta H^f_{\mathrm{CVAs}}=-0.69$ eV. This indicates that the C*V*As complex is energetically more favorable than the substitutional dopant. In order to compare this result with the stability of C*V*P and C*V*Sb complexes, we assume that the pre-exponential factor C' is independent of the dopant element. Within this constraint we obtain $\Delta H^f_{\mathrm{CVP}}=-0.77$ eV ($\Delta H^f_{\mathrm{CVSb}}=-0.85$ eV). Assuming that the formation enthalpies of the substitutional donors are roughly the same, the difference between the values of $\Delta H^f_{\mathrm{CVA}}$ for the various dopants gives a hint on the stability of the C*VA* complexes,

$$\Delta H^f_{\mathrm{CVP}} - \Delta H^f_{\mathrm{CVAs}} = -0.08 \text{ eV}, \quad (16)$$

$$\Delta H^f_{\mathrm{CVSb}} - \Delta H^f_{\mathrm{CVAs}} = -0.16 \text{ eV}, \quad (17)$$

$$\Delta H^f_{\mathrm{CVSb}} - \Delta H^f_{\mathrm{CVP}} = -0.08 \text{ eV}. \quad (18)$$

C*V*Sb is the most stable complex among C*VA* with $A\in\{\mathrm{P,As,Sb}\}$ and the stability of C*VA* increases according to the sequence As→P→Sb. Theoretical calculations on the binding energies of C*VA* complexes with respect to the isolated point defects are reported by Chroneos *et al.*[17] Binding energies $H^b_X=-0.60$, -0.66, and -0.85 eV were obtained for $X=$C*V*P, C*V*As, and CSb*V*, respectively, with energy differences

$$H^b_{\mathrm{CVP}} - H^b_{\mathrm{CVAs}} = 0.06 \text{ eV}, \quad (19)$$

$$H^b_{\mathrm{CSb}V} - H^b_{\mathrm{CVAs}} = -0.19 \text{ eV}, \quad (20)$$

$$H^b_{\mathrm{CSb}V} - H^b_{\mathrm{CVP}} = -0.25 \text{ eV}. \quad (21)$$

The calculations confirm the experimental observation that complexes with Sb are more stable than complexes with P and As. The energy differences deduced from the experimental results [see Eqs. (16)–(18)] and the theoretical calculations [see Eqs. (19)–(21)] are of the same order of magnitude. However, theory predicts a stability of the C*VA* complexes that increases according to the sequence P→As →Sb and hence is at variance with the experiment. This difference is likely caused by the assumptions considered to arrive at Eqs. (16)–(18) and not due to the accuracy of the theoretical calculations. Theory provides additional structural information on the complex that is not accessible by the diffusion experiment. The calculations show that a CSb*V* complex with an Sb atom next to carbon and a vacancy rather than a C*V*Sb complex is more bound (see Part II).

The theoretical calculations performed so far do not provide any information about the charge state of the triple-defect clusters. The experiments on the simultaneous self-diffusion and dopant diffusion, however, indicate that the clusters must be neutral rather than positively or negatively charged. This becomes evident with the gradual reduction in the self-diffusion coefficient with increasing dopant penetration depth. The change in self-diffusion across the isotope structure correlates with the concentration profile of the substitutional donor. No evidence of additional *n*- or *p*-type doping within the C-doped ^{70}Ge layers due to the formation of charged triple-defect clusters is found.

Evidence for the formation of As complexes that are not related to C stems from the shape of the dopant profiles both in natural and isotopically enriched Ge. In particular, the P and As profiles are less box shaped than those predicted by vacancy mechanism (1).[40] Assuming that the total concentration of P and As is electrically active, the diffusion induced broadening of the Ge isotope structure should be more pronounced than observed experimentally. This and the fact that the interference between self-diffusion and dopant diffusion is accurately described when reaction (3) is taken into account give indirect evidence for the formation of donor-vacancy clusters. In this respect, it is worth to note that both As and P profiles measured by means of the spreading-resistance technique exhibit the expected box shape and, accordingly, are accurately described on the basis of vacancy mechanism (1).[11] Obviously, the differences between the electrical and chemical dopant profiles must be due to neutral dopant-related complexes. These observations led us to assume reaction (3) that basically describes the formation of a neutral A_2V complex via Coulomb attraction between the negatively charged donor-vacancy pair and the positively charged substitutional dopant. In fact, theory predicts the formation of e.g., As_nV clusters with $n\in\{1,2,3,4\}$ (Ref. 16) as well as P_nV clusters with $n\in\{1,2,3,4\}$ and Sb_nV clusters with $n\in\{1,2,3,4,5\}$ (see Part II). The clusters with the maximum binding energies are P_4V, As_4V, and Sb_5V. The clusters P_4V and As_4V prevail at temperatures below 800 K, but for temperatures exceeding 900 K theory predicts that A_2V clusters are more significant for $A\in\{\mathrm{P,As}\}$. Therewith, our assignment of the donor-vacancy cluster to the A_2V defects is supported by theory (see Part II). According to the calculations the configuration is *AVA* with $A\in\{\mathrm{P,As}\}$, i.e., a vacancy with two nearest-neighbor P (As) atoms rather than PP*V* (AsAs*V*) with one P (As) atom in nearest-neighbor position and another in a second-nearest-neighbor position to the vacancy.[16,18] So far, predictions on the charge states of As-vacancy clusters are not available for a comparison.

The continuum theoretical simulations of Sb diffusion in Ge show that the formation of Sb-vacancy clusters do not significantly affect the doping of Ge and the diffusion of Sb. This probably holds only for low Sb doping levels realized in our diffusion experiments. Following the theoretical calculations of Coutinho *et al.*,[19] Sb-related clusters are predicted to compensate for Sb donors. Such clusters are likely formed after high-dose Sb implantation in subsequent anneals for dopant activation. The calculations reported in Part II also reveal a higher stability of Sb-related clusters with and without C compared to the corresponding P- and As-related defects. However, in our experiments the formation of Sb_nV clusters is very likely kinetically suppressed compared to the formation of CSb*V* clusters, because the Sb doping level is low and Sb_2V complexes that may act as precursor for more complex clusters are less mobile than Sb*V* pairs (see Part II). Accordingly, the high C concentration in our Ge structures and high mobility of Sb*V* pairs favor the formation of CSb*V* complexes rather than that of Sb_nV clusters.

Finally, the different settings assumed for the effective C concentration $C^{\mathrm{eff}}_{\mathrm{C}}$ are discussed. Accurate modeling of Sb

and P diffusion in the heavily C-doped isotope structure requires values of 3.7×10^{19} and 1.3×10^{20} cm^{-3}, respectively. Modeling of As diffusion points to C_C^{eff} data that range between 3.5×10^{19} and 7.0×10^{19} cm^{-3} for temperatures between 600 and 700 °C. The different settings of C_C^{eff} may indicate that a limited amount of C is an effective trapping center and that this amount depends on the type of the dopant. However, one may also argue that the amount of efficient trapping centers is independent of the dopant. In this case, the different values of C_C^{eff} indicate that not only C*VA* but also C$(VA)_n$ complexes are formed. Assuming that the effective trap concentration of 3.7×10^{19} cm^{-3} serves for the formation of C*V*Sb, $C_C^{eff}=1.3\times10^{20}$ cm^{-3} determined for P could then be related to the formation of C$(VP)_3$. Following this interpretation, the temperature dependence of C_C^{eff} observed for the case of As may suggest the formation of C$(V\mathrm{As})_2$ complexes, whose contribution increases with temperature at the expense of C*V*As formation. In fact, the theoretical calculations presented in Part II show that the trapping of an extra *AV* pair by a C*VA* cluster leads to a strong increase in the binding energy. Therewith the formation of more complex C$(AV)_n$ clusters is quite realistic.

V. CONCLUSIONS

The diffusion experiments of the *n*-type dopants *A* with $A\in\{\mathrm{P,As,Sb}\}$ in Ge isotope multilayer structures doped with the isovalent impurity carbon provide comprehensive information on the mechanisms and the properties of the atomic defects involved in the matter transport. The simultaneous diffusion of dopants and self-atoms reveal that the vacancy in Ge is doubly negatively charged even under electronically intrinsic conditions. Recent experiments on the intrinsic and extrinsic diffusion of the *n*-type dopants in Ge demonstrate that singly negatively charged donor-vacancy pairs control the diffusion of the dopants and are responsible for the observed strong enhancement of diffusion under extrinsic doping conditions.[11] From the activation enthalpy of dopant diffusion, we conclude that the binding energy of $(AV)^-$ pairs increases with increasing size of the dopant element. Within the approach of Dunham and Hu,[38] the differences in the binding energy of *AV* pairs describe a shift in the potential energy landscape of the vacancy diffusion pathway in the neighborhood of the dopant. This shift is a consequence of the local stress in the Ge matrix due to the different sizes of the dopants. The local stress around an oversized isolated dopant is effectively reduced by pairing of the dopant with a vacancy. Elastic interactions also explain the diffusion of the isovalent impurity tin (Sn) in the Si-Ge alloy system[41] and the preferred Sn-split-vacancy configuration[42] compared to the substitutional Sn-vacancy configuration in Si and Ge.

The enhanced diffusion of the *n*-type dopants P, As, and Sb under extrinsic conditions is strongly retarded by doping of Ge with the isovalent impurity carbon. Carbon can be incorporated by epitaxial deposition techniques to concentrations several orders of magnitude above its solubility limit.[23] Continuum theoretical calculations of the complex behavior of dopant diffusion in Ge isotope multilayer structures doped with C reveals that the trapping of the mobile charged dopant-vacancy pairs leads to the formation of neutral complexes. These complexes are considered to consist of one carbon, one dopant, and a vacancy. The undersized substitutional C_s produces large tensile strain that attracts the mobile donor-vacancy pair but not the doubly negatively charged vacancy; i.e., self-diffusion is not affected by the presence of C. The stability of C*VA* complexes and instability of C*V* pairs is confirmed by recent density-functional theory calculations of Chroneos *et al.*[17]

Additional defect complexes become evident at high dopant concentrations in high-purity Ge. Whereas for maximum dopant concentrations of about 10^{19} cm^{-3} dopant diffusion is accurately described on the basis of the vacancy mechanism, the shape of the dopant profiles obtained for concentrations above 10^{19} cm^{-3} is at variance with the vacancy mechanism. Accurate simulations of the experimental diffusion profiles require the existence of neutral dopant-defect complexes that form due to the Coulomb attraction between the singly negatively dopant-vacancy pair $(AV)^-$ and the singly positively charged substitutional dopant A_s^+. The stability of these A_2V complexes is confirmed by the theoretical calculations in Part II. Overall, Eqs. (1)–(3) represent the minimum system of diffusion reactions that are required to accurately model the complex diffusion of *n*-type dopants in C-doped Ge at low and high doping levels. The theoretical calculations presented in Part II confirm the stability of the defects involved in reactions (1)–(3) and therewith provide additional evidence for these reactions.

The good agreement between the experimental results and theoretical predictions on the binding energies of *AV* pairs and C*VA* complexes proves vacancy mechanism (1) and reactions (2) and (3) for modeling the diffusion of the *n*-type dopants P, As, and Sb in Ge. It is interesting to note that in the case of Si, no agreement between experiment and theory exists on dopant diffusion and even self-diffusion via the vacancy mechanism.[40] The reason for this discrepancy that is fundamental for our understanding on atomic transport in Si and SiGe will be discussed in a separate paper.[43]

For the fabrication of modern electronic nanodevices, the enhanced diffusion of *n*-type dopants observed under electronically extrinsic conditions and the deactivation of donors at high dopant concentrations hinder the formation of ultrashallow junctions with high active dopant concentrations. The enhanced diffusion of the dopants can be effectively suppressed by an incorporation of C. Like in the case of B, it is very likely that a high concentration of C can be incorporated on substitutional sites by ion implantation and subsequent anneals to remove the implantation damage. However, the deactivation problem of the *n*-type dopants at high doping levels is not solved by C. In order to control the formation of neutral or even acceptor-like dopant-vacancy complexes that compensate for the donors, other concepts must be considered. In this respect, Ge self-interstitials would be extremely helpful, since in the case they can be introduced in supersaturation, they would suppress not only the formation of dopant-defect complexes but also the formation of dopant-vacancy pairs and thus would suppress both the diffusion and the deactivation of *n*-type dopants. Defect engineering with Ge self-interstitials could solve the problems associated with

the fabrication of Ge-based *n*-channel metal-oxide-semiconductor field-effect transistors (*n*-MOSFET's). However, isolated Ge interstitials have not yet been observed in experiment either directly or indirectly. But interstitial-type {113} defects have been found after hydrogen and P implantation in Ge.[44,45] Additional efforts are still required to create and control the formation of isolated interstitials and more complex interstitial-type defects. In this respect, experiments on radiation enhanced diffusion of self-atoms and dopant atoms can help to determine the properties of Ge interstitials.[20] Early attempts indicate an enhancement of P diffusion in Ge under proton irradiation.[46] This enhancement is associated with the supersaturation of vacancies formed by proton irradiation that lead to enhanced concentrations of mobile P*V* pairs compared to their concentrations under thermal equilibrium conditions. In order to investigate, in particular, the properties of isolated Ge self-interstitials, the radiation enhanced diffusion of foreign atoms must be considered that mainly diffuse by means of self-interstitials. Both B- or C-doped Ge isotope structures are suitable test structures for radiation enhanced self-diffusion and dopant diffusion experiments. These experiments could help to determine the properties of Ge self-interstitials. This information is of fundamental significance to utilize this defect for effective defect engineering in the fabrication of *n*-MOSFET's.

ACKNOWLEDGMENTS

This work was supported by the Deutsche Forschungsgemeinschaft under Reference No. Bra 1520/6-1. We thank A. Chroneos of the Imperial College London for valuable discussions, I. Romandic and A. Theuwis (Umicore, Olen, Belgium) for donating low doped *p*-type Ge wafers for diffusion experiments in natural Ge, and T. Clarysse for the nanospreading resistance measurements. The work at UC Berkeley was supported by U.S. NSF Grant No. DMR-04-05472.

*bracht@uni-muenster.de

[1] *Germanium-Based Technologies—From Materials to Devices*, edited by C. Claeys and E. Simoen (Elsevier, Amsterdam, 2007).

[2] C. O. Chui, K. Gopalakrishnan, P. B. Griffin, J. D. Plummer, and K. C. Saraswat, Appl. Phys. Lett. **83**, 3275 (2003).

[3] A. Satta, E. Simoen, T. Clarysse, T. Janssens, A. Benedetti, B. De Jaeger, M. Meuris, and W. Vandervorst, Appl. Phys. Lett. **87**, 172109 (2005).

[4] Y. S. Suh, M. S. Carroll, R. A. Levy, G. Bisognin, D. De Salvador, and M. A. Sahiner, *Progress in Semiconductor Materials V—Novel Materials and Electronics and Optoelectronic Applications*, MRS Symposia Proceedings No. 891 (Materials Research Society, Pittsburgh, 2006), p. EE7.20.1.

[5] A. Satta, E. Simoen, R. Duffy, T. Janssens, T. Clarysse, A. Benedetti, M. Meuris, and W. Vandervorst, Appl. Phys. Lett. **88**, 162118 (2006).

[6] A. Satta, T. Janssens, T. Clarysse, E. Simoen, M. Meuris, A. Benedetti, I. Hoflijk, B. De Jaeger, C. Demeurisse, and W. Vandervorst, J. Vac. Sci. Technol. B **24**, 494 (2006).

[7] G. Luo, C.-C. Cheng, C.-Y. Huang, S.-L. Hsu, C.-H. Chien, W.-X. Ni, and C.-Y. Chang, Electron. Lett. **41**, 1354 (2005).

[8] A. Chroneos, D. Skarlatos, C. Tsamis, A. Christofi, D. S. McPhail, and R. Hung, Mater. Sci. Semicond. Process. **9**, 640 (2006).

[9] M. S. Carroll and R. Koudelka, Semicond. Sci. Technol. **22**, S164 (2007).

[10] H. Bracht and S. Brotzmann, Mater. Sci. Semicond. Process. **9**, 471 (2006).

[11] S. Brotzmann and H. Bracht, J. Appl. Phys. **103**, 033508 (2008).

[12] S. Uppal, A. F. W. Willoughby, J. M. Bonar, N. E. B. Cowern, T. Grasby, R. J. H. Morris, and M. G. Dowsett, J. Appl. Phys. **96**, 1376 (2004).

[13] B. J. Pawlak, R. Duffy, T. Janssens, W. Vandervorst, S. B. Felch, E. J. H. Collart, and N. E. B. Cowern, Appl. Phys. Lett. **89**, 062102 (2006).

[14] P. A. Stolk, H. J. Gossmann, D. J. Eaglesham, and J. M. Poate, Mater. Sci. Eng., B **36**, 275 (1996).

[15] J. Coutinho, V. J. B. Torres, S. Öberg, A. Carvalho, C. Janke, R. Jones, and P. R. Briddon, J. Mater. Sci.: Mater. Electron. **18**, 769 (2007).

[16] A. Chroneos, R. W. Grimes, B. P. Uberuaga, S. Brotzmann, and H. Bracht, Appl. Phys. Lett. **91**, 192106 (2007).

[17] A. Chroneos, B. P. Uberuaga, and R. W. Grimes, J. Appl. Phys. **102**, 083707 (2007).

[18] A. Chroneos, R. W. Grimes, and C. Tsamis, J. Mater. Sci.: Mater. Electron. **18**, 763 (2007).

[19] J. Coutinho, C. Janke, A. Carvalho, S. Öberg, V. J. B. Torres, R. Jones, and P. R. Briddon, Defect Diffus. Forum **273-276**, 93 (2008).

[20] S. Schneider, H. Bracht, M. C. Petersen, J. Lundsgaard Hansen, and A. Nylandsted Larsen, J. Appl. Phys. **103**, 033517 (2008).

[21] M. Werner, H. Mehrer, and H. D. Hochheimer, Phys. Rev. B **32**, 3930 (1985).

[22] E. E. Haller, W. L. Hansen, P. Luke, R. McMurray, and B. Jarrett, IEEE Trans. Nucl. Sci. **29**, 745 (1982).

[23] J. D'Arcy-Gall, D. Gall, I. Petrov, P. Desjardins, and J. E. Greene, J. Appl. Phys. **90**, 3910 (2001).

[24] T. Clarysse, P. Eyben, T. Janssens, I. Hoflijk, D. Vanhaeren, A. Satta, M. M. Meuris, W. Vandervorst, J. Bogdanowicz, and G. Raskin, J. Vac. Sci. Technol. B **24**, 381 (2006).

[25] V. P. Markevich, I. D. Hawkins, A. R. Peaker, K. V. Emtsev, V. V. Emtsev, V. V. Litvinov, L. I. Murin, and L. Dobaczewski, Phys. Rev. B **70**, 235213 (2004).

[26] V. P. Markevich, A. R. Peaker, V. V. Litvinov, V. V. Emtsev, and L. I. Murin, J. Appl. Phys. **95**, 4078 (2004).

[27] C. E. Lindberg, J. Lundsgaard Hansen, P. Bomholt, A. Mesli, K. Bonde Nielsen, A. Nylandsted Larsen, and L. Dobaczewski, Appl. Phys. Lett. **87**, 172103 (2005).

[28] A. R. Peaker, V. P. Markevich, F. D. Auret, L. Dobaczewski, and N. Abrosimov, J. Phys.: Condens. Matter **17**, S2293 (2005).

[29] J. Coutinho, S. Öberg, V. J. B. Torres, M. Barroso, R. Jones, and P. R. Briddon, Phys. Rev. B **73**, 235213 (2006).

[30] A. Fazzio, A. Janotti, A. J. R. da Silva, and R. Mota, Phys. Rev. B **61**, R2401 (2000).

[31] J. Coutinho, R. Jones, V. J. B. Torres, M. Barroso, S. Öberg, and P. R. Briddon, J. Phys.: Condens. Matter **17**, L521 (2005).
[32] E. Simoen, A. Satta, A. D'Amore, T. Janssens, T. Clarysse, K. Martens, B. De Jaeger, A. Benedetti, I. Hoflijk, B. Brijs, M. Meuris, and W. Vandervorst, Mater. Sci. Semicond. Process. **9**, 634 (2006).
[33] K. Saarinen, J. Nissilä, H. Kauppinen, M. Hakala, M. J. Puska, P. Hautojärvi, and C. Corbel, Physica B (Amsterdam) **273-274**, 463 (1999).
[34] V. Ranki and K. Saarinen, Physica B (Amsterdam) **340-342**, 765 (2003).
[35] V. V. Emtsev, T. V. Mashovets, and S. M. Ryvkin, Inst. Phys. Conf. Ser. **16**, 17 (1973).
[36] S. N. Abdurakhmanova, T. N. Dostkhodzhaev, V. V. Emtsev, and T. V. Mashovets, Sov. Phys. Semicond. **8**, 1771 (1974).
[37] S. M. Hu, Phys. Status Solidi B **60**, 595 (1973).
[38] S. T. Dunham and C. D. Wu, J. Appl. Phys. **78**, 2362 (1995).
[39] A. Chroneos, H. Bracht, R. W. Grimes, and B. P. Uberuaga, Appl. Phys. Lett. **92**, 172103 (2008).
[40] H. Bracht, Phys. Rev. B **75**, 035210 (2007).
[41] I. Riihimäki, A. Virtanen, H. Kettunen, P. Pusa, P. Laitinen, J. Räisänen, and ISOLDE Collaboration, Appl. Phys. Lett. **90**, 181922 (2007).
[42] H. Höhler, N. Atodiresei, K. Schroeder, R. Zeller, and P. H. Dederichs, Phys. Rev. B **71**, 035212 (2005).
[43] H. Bracht and A. Chroneos (unpublished)
[44] M. L. David, F. Pailloux, D. Babonneau, M. Drouet, J. F. Barbot, E. Simoen, and C. Claeys, J. Appl. Phys. **102**, 096101 (2007).
[45] M. L. David and F. Pailloux (unpublished)
[46] R. L. Minear, D. G. Nelson, and J. F. Gibbons, J. Appl. Phys. **43**, 3468 (1972).